Solar-Terrestrial Physics, 2016. Vol. 2. Iss. 2, pp. 15–27, DOI: 10.12737/20996. © INFRA-M Academic Publishing House
Original Russian version D.A. Zhdanov, S.V. Lesovoi, S.Kh. Tokhchukova, published in Solnechno-Zemnaya Fizika. 2016, vol. 2, iss. 2, pp. 12–21, DOI 10.12737/17341

SOURCES OF TYPE III SOLAR MICROWAVE BURSTS

D.A. Zhdanov[1], S.V. Lesovoi[1], S.Kh. Tokhchukova[2]

Institute of Solar-Terrestrial Physics SB RAS, Irkutsk, Russia, zhdanov@iszf.irk.ru
Special Astrophysical Observatory RAS, Saint-Petersburg, Russia, stokh@mail.ru

---

Microwave fine structures allow us to study plasma evolution in an energy release region. The Siberian Solar Radio Telescope (SSRT) is a unique instrument designed to examine fine structures at 5.7 GHz. A complex analysis of data from RATAN-600, 4–8 GHz spectropolarimeter, and SSRT, simultaneously with EUV data, made it possible to localize sources of III type microwave bursts in August 10, 2011 event within the entire frequency band of burst occurrence, as well as to determine the most probable region of primary energy release. To localize sources of III type bursts from RATAN-600 data, an original method for data processing has been worked out. At 5.7 GHz, the source of bursts was determined along two coordinates, whereas at 4.5, 4.7, 4.9, 5.1, 5.3, 5.5, and 6.0 GHz, their locations were identified along one coordinate. The size of the burst source at 5.1 GHz was found to be maximum as compared to those at other frequencies.

Keywords: *Type III microwave bursts, fine structures, solar microwave emission.*

INTRODUCTION

Radio observations of solar flares show that along with typical microwave bursts there are narrowband bursts called fine structures [Droege, 1977; Benz, 1986; Staehli et al., 1987; Allaart et al., 1990; Bruggmann et al., 1990; Altyntsev et al., 1999; Jiricka et al., 2001; Chernov et al., 2003; Fu et al., 2004; Huang et al., 2010; Zhdanov et al., 2015]. The narrow fractional bandwidth less than 5 % and subsecond lifetimes impose severe restrictions on source sizes and emission processes. The variety of temporal and spectral features of fine structures points both to different mechanisms for emission generation and to various conditions of energy release from a generation region. These features have been studied well enough, but literature contains very little information about their sources or lacks it at all because most spectral observations were not accompanied by spatial observations.

In the middle 1990s, no high spectral resolution observations were performed near the SSRT operating frequency (5.7 GHz) [Altyntsev et al., 1996]. This seriously hindered adequate interpretation of subsecond bursts observed at SSRT which were then called subsecond pulses (SSP). Evolving technologies of extensive data transfer made it possible to use data from solar spectrometers located in Chinese observatories [Fu et al., 1995]. The data agreed in time and frequency (5.2–7.6 GHz) with SSRT observations. Early studies [Sych et al., 2002; Meshalkina et al., 2002; Altyntsev et al., 2003; Meshalkina et al.,

2004] have revealed that SSP in dynamic spectra correspond to different spectral structures. In [Meshalkina et al., 2002; Altyntsev et al., 2007; Meshalkina et al., 2012] structures called type III microwave bursts [Staehli et al., 1987] were examined.

It is certainly important to know about location of fine structure sources and their sizes to specify the emission mechanism and to determine plasma parameters in the emission region [Chernov et al., 2014]. Unfortunately, there are no radio telescopes in the world able to directly localize sources of microwave fine structures in a broad bandwidth. Such instruments are still under development [Yan et al., 2013; Lesovoi et al., 2014; Gary et al., 2014].

Existing spectropolarimeters have high spectral (to 5 MHz) and temporal (to 5 ms) resolution, but have no spatial resolution [Fu et al., 1995; Zhdanov et al., 2011]. Radioheliographs, in particular SSRT (5.7 GHz) [Grechnev et al., 2003] and Nobeyama (17 and 34 GHz) [Nakajima et al., 1994] having high spatial resolution (to 10″) make observations only in one or two fixed frequencies. Thus, RATAN-600 observations provide unique information about spatial-frequency features of fine structure sources.

The analysis of the data archive for RATAN-600 (the interval of daily observations is 07–11 UT) and for the 4–8 GHz spectropolarimeter (the interval is 00–10 UT) from March 2011 to June 2013 has shown that RATAN-600 registered only four of 79 events with fine structure observed by the spectropolarimeter between 07 and 10 UT: August 10, 2011 at 09:34 UT; June 29, 2012 at 09:13 UT; July 14, 2012 at 07:35 UT; and March 22, 2013 at 08:39 UT. The small number of identical observations is explained by the transit mode of RATAN-600.

In this paper, we present results obtained from the analysis of radio data on the August 10, 2011 event. To localize fine structure sources, we examine data from RATAN-600, 4–8 GHz spectropolarimeter, and SSRT. We have devised a unique method for localizing fine structure sources. It enabled us to find a 2D position of a type III microwave burst source at 5.7 GHz as well as 1D positions of sources at other frequencies. We established that the size of type III microwave burst sources was maximum at 5.1 GHz. EUV data from SDO/AIA showed that the sources were situated along interacting loops seen in extreme ultraviolet (EUV).

INSTRUMENTS

The 4–8 GHz spectropolarimeter (Badary Broadband Microwave Spectropolarimeter, BBMS) – a 26 channel modulation straight receiver operating in a bandwidth 3.8–8.2 GHz [Zhdanov et al., 2011; Zhdanov et al., 2015] – is installed in the Radio Astrophysical Observatory of the Institute of Solar-Terrestrial Physics SB RAS. We acquired spectral data, using a filter bank with each filter channel spaced in frequency from the next one by 120 MHz on average. The pass band of each filter is less than 30 MHz. Temporal resolution of stored data is 10 ms with flux sensitivity of about 1 sfu. The observation data are presented as curves of integral fluxes at 26 frequencies in two circular polarizations. BBMS has made regular observations since August 2010.

The Siberian Solar Radio Telescope (SSRT) is a cross-shaped interferometer operating at a frequency of 5.7 GHz [Grechnev et al., 2003]. It receives signals in both circular polarizations. The interferometer is comprised of two linear equidistant antenna arrays oriented north–south (NS) and east–west (EW); each array consists of 128 antennae. Spatial resolution generally depends on width and relative angular position of EW and NS knife-edge patterns. Typical spatial resolution in 2D mode is 21″; in 1D mode, 15″. Temporal resolution for a 2D image is 2–3 min; for 1D mode, 14 ms (7 ms for each polarization). To take a 2D image, we employ the method of frequency scanning with due regard to the diurnal Earth rotation. We perform frequency scanning by recording the power spectrum of a signal at 5.67–5.79 GHz at the output of the interferometer with a 500-channel spectrum analyzer – an acousto-optic receiver. The resulting signal from all the channels is an instantaneous 1D angular distribution of radio brightness.

The radio telescope of the Russian Academy of Sciences (RATAN-600) is a transit radio telescope about 600 m in diameter located in Zelenchukskaya station [Khaikin et al., 1972; Bogod et al., 2004]. It observes the Sun in the southern sector with a flat reflector; together they make up a periscope system. RATAN-600 detects solar emission in a frequency range from 750 MHz to 18.2 GHz [Bogod et al., 2011a]. Solar observations are 1D images (scans) captured when the Sun passes through a fixed knife-edge pattern. In the multi-azimuthal regime of observations, the number of solar scans per day increased from one to 61 [Bogod et al., 2011a]. The observations are made near local noon from 7 to 11 UT. The interval between observations (between adjacent azimuths) can be around 4–8 min. This enables us to study the dynamics of solar formations on time scales minutes–hours, as well as to register flare events at different stages of their development [Bogod, 2011b].

The cadence at each frequency is up to 14 ms. Spatial resolution depends on the received frequency; and accurate within 10 % the beam size in angular minutes can be estimated as $250\,f^{-1}$ with f being a frequency in GHz [Tokhchukova et al., 2014]. Table gives more exact beam sizes with respect to the opening angle of spiral feeds employed in this period.

In 2005–2011, different spiral feeds received right- and left-hand circular polarizations. Offset of the feed relative to the focus for each of the polarizations was 17.5 mm.

DATA ANALYSIS

We study the C2.4 (GOES) solar flare that occurred on August 10, 2011 at 09:36 UT. This event is discussed in [Kashapova et al., 2013a; Kashapova et al., 2013b]. The authors show that RATAN-600 and BBMS observed the SSP simultaneously. They analyzed the correlation between curves of radio fluxes, X-ray fluxes, evolution of electron temperature, and emission measure, and assumed that the nature of the SSP and flare was generally related to a high-temperature source.

Nevertheless, the question about the origin of SSP in this event remained open because the source was not localized. The matter is that the standard method for localizing SSP sources from SSRT data requires

data from two antenna arrays [Meshalkina et al., 2002; Altyntsev et al., 2003], but only the EW array is capable to observe the Sun due to features of the SSRT beam pattern [Grechnev et al., 2003]. However, we can use RATAN-600 data to determine the second coordinate of the position of the burst source at 5.7 GHz.

Figure 1 illustrates dynamic spectra of this event and RATAN-600 1D data at 5.7 GHz. In the interval 09:34:40–09:34:50 UT, SSP are identified with type III drift microwave bursts observed in a bandwidth from 4.5 to 6 GHz.

The analysis of EW data showed that the radio brightness center associated with a continual source was displaced relative to its initial position (Figure 2, *a*, *b*). Note that we averaged available EW data only to 0.3 s. In the source SSRT record, to the continual source corresponds a continuous dark stripe with sizes up to 80″; and SSP against the continual source look like short-duration compact very dark cores. Notice that microwave light curves (Figure 2, *d*, *e*) distinguish three groups of drift bursts. We consider each of these groups as a separate cluster of the event. RATAN-600 registered only one group at 09:34:40–09:34:50 UT.

Taking the preflare position of the continual source to be the origin of relative coordinates, we have established that the center of the response to the drifting burst source shifted by 20″ from the preflare position of the continual source. In the following, in terms of relative shifts we will discuss one-dimensional data associated with radio maps at the same frequencies.

The full width at half maximum (FWHM) of the observed response behaves oppositely to the flux (see Figure 2, *c*). In fact, during the drifting bursts the size of the response decreased by 70″ in all the three groups, whereas after each of the clusters the continual source regained its original size. We may assume that a more compact and intense pulse source existed near the continual one; therefore, the pulse source was more effective for the observed response.

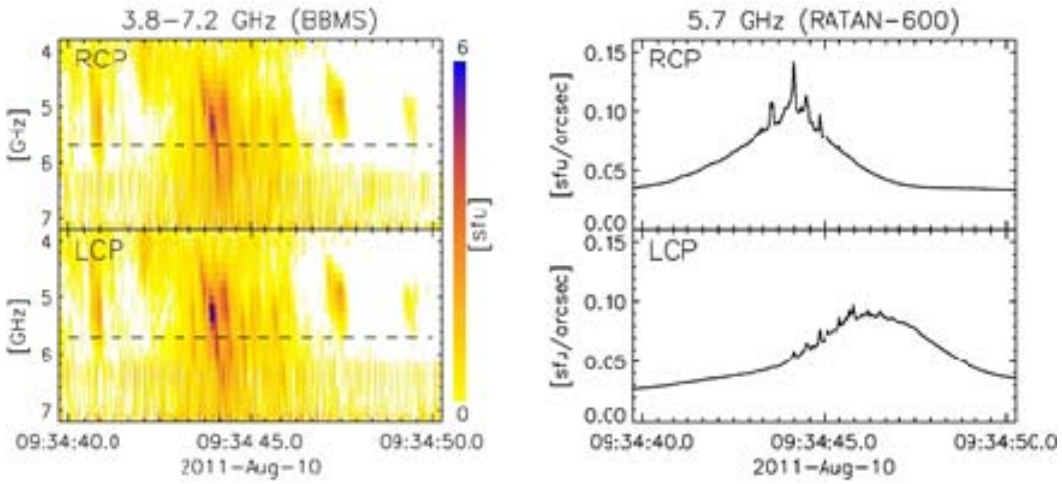

Figure 1. Type III microwave bursts in the August 10, 2011 event. On the left are dynamic spectra 3.8–7.2 GHz (BBMS) between 09:34:40–09:34:50 UT. Horizontal dashed lines indicate the frequency of 5.7 GHz. On the right are RATAN-600 scans at 5.7 GHz in the same interval

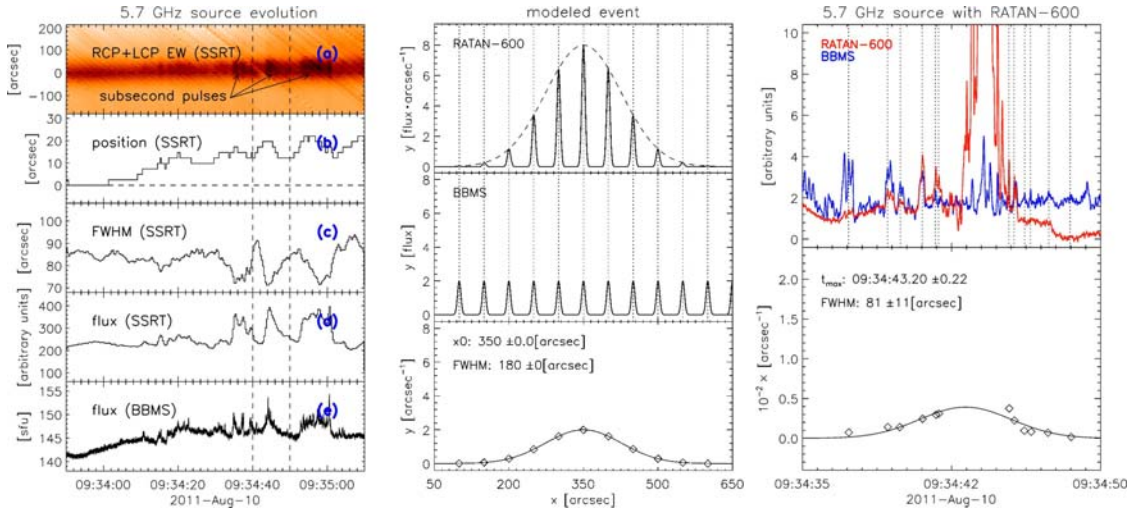

Figure 2. 1D position of the source at 5.7 GHz. Left panels present SSRT data; the center, simulation results; the right panels, the result of RATAN-600 data processing by the original method at 5.7 GHz. Panel *a* shows the source recording from the EW array with a temporal resolution of 0.3 s; the continual source is the dark stripe over the entire interval; arrows mark clusters of subsecond pulses (SSP). The width of the EW array diagram is 35″. On the next panels are curves describing the evolution of the location of the radio brightness center (*b*), the size (*c*), the radio flux from the source (*d*), and the integral flux (*e*). The solid curve depicts the reconstructed response in RATAN-600 data simulation and processing. The dashed curve represents an approach to the beam pulse amplitude modulation. Dotted vertical lines indicate pulses used to reconstruct the response. Diamonds are the values after normalization. The time profiles of RATAN-600 (red curve) and BBMS (blue curve) contain only a quickly varying component

We have found out that according to SSRT data the positions of SSP sources in the right-hand (RCP) and left-hand (LCP) circular polarizations coincide; therefore, in what follows we consider only RCP. Panel *a* in Figure 2 presents data from the EW array in intensity (RCP+LCP).

We can find the second coordinate of a drifting burst source from RATAN-600 1D data. Figure 1 (on the right) shows that LCP and RCP scans shift in time with respect to each other. This effect is explained by characteristics of RATAN-600 that is equipped with two feeds placed outside of the focus so that an angular distance between beam centers is 37.6″ (or 2.5 s in time with due regard to the Earth rotation). Thus, the continual emission source passed through the RCP beam center earlier than through the LCP beam center.

It is known that the observed response size should be more than the beamwidth of the antenna pattern. On the other hand, we have established that the observed RATAN-600 response contained pulses with corresponding sizes smaller than the beamwidth. This fact can explain why the lifetime of the pulse source was shorter than the period during which it moved through the antenna beam pattern. In our case, angular sizes of some pulses with a mean lifetime of 0.2 s are within 3″, being thus approximately 10 times smaller than the beamwidth of the RATAN-600 at 5.7 GHz (44″). In this case, the response (scan) obtained by the transit instrument is not convolution of antenna pattern with angular distribution of radio brightness. To reconstruct the scan, we should have some prior information about behavior of emitting source. Thus, if the

pulse source holds its size but radio brightness changes with time, we can reconstruct the scan as it was before the convolution of radio brightness distribution over the source with beam pattern.

For example, we simulate RATAN-600 observations of an ideal source generating bursts with the same amplitude (Figure 2, central panels). The amplitude of each pulse depends on the position of the source relative to beam maximum and on the true pulse amplitude. As a result, all the pulses are below the dashed curve being a response to the source of these pulses.

Hence, knowing pulse amplitudes in the integral flux, we can reconstruct the response. For example, we can use BBMS data to find pulse amplitudes. Bottom central panel on Figure 2 shows the required response to the source obtained by normalizing the RATAN-600 scan by the integral flux during pulses. Using the proposed method, we localized the source at 5.7 GHz from RATAN-600 data (Figure 2, right panels).

Notice that in real observations it is necessary to compare only pulse-induced increments without slowly varying components. In the integral flux, we found the background as a running mean with a window exceeding the duration of separate bursts. The background in the RATAN-600 scan was subtracted in two iterations. First, we subtracted the preflare scan in azimuth –2 from the flare scan in azimuth –4. Then, we subtracted the test profile of the unknown flare continual source. Nevertheless, we failed to separate all pulses from the background; therefore, we normalized scans by bursts located on edges of the scans. In Figure 3, the pulses used to reconstruct the response are marked with vertical dashed lines.

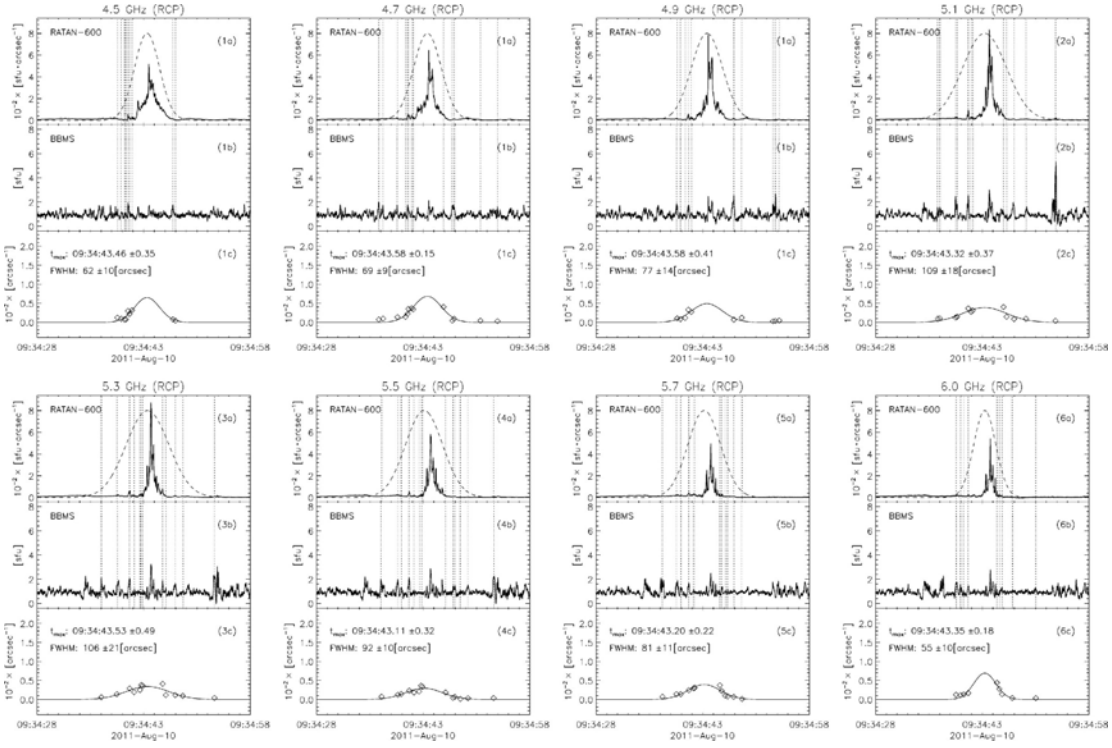

Figure3. Localization of burst sources by the method of normalization at eight frequencies in RCP

As alternative methods for subtracting the background, we can employ a Fourier filter in order to filter low harmonics or to try to describe the background by a polynomial passing through the set of minima between bursts.

Frequency correspondence. Sizes and relative positions of sources

RATAN-600 (MHz)	4500	4700	4900	5100	5300	5500	5700	6000
BBMS (MHz)	4454	4687	4886	5026	5398	5494	5744	5957
SSRT[1] (MHz)	–	–	–	–	–	–	5700	–
RATAN-600 beam (arcsec)	50	48	45	44	43	41	40	38
Response (arcsec)	62±10	69±9	77±14	109±18	106±21	92±10	81±11	55±10
Source (arcsec)	37	50	62	100	97	82	70	40
Displacement (arcsec)	–14±5	–16±2	–16±6	–12±6	–15±7	11±5	10±3	–12±3

Note: beam is 35″; response, 70″; source, 61″

To apply this method, we should pay special attention to the background subtraction in RATAN-600 scans. Otherwise, normalization yields a response to the continual source, not to the fine structure source because the increment of the radio flux from the continual source is much larger than that from the drifting burst source. In the case of significant and abrupt changes in the radio flux amplitude caused by microwave bursts, the background subtraction in RATAN-600 scans requires a nontrivial solution.

We can utilize the proposed method to determine the 1D position of the response not only at 5.7 GHz but also at any other frequency at which RATAN-600 and BBMS observed the drift bursts. Since these instruments have different sets of frequencies, for the analysis we have selected only close ones. As a result, we found responses to the sources of the drift bursts of interest at eight frequencies (Table and Figure 3).

Note that the reconstructed responses should be larger than or equal to the beamwidth; and all pulses should be inside a response – otherwise the reconstruction is wrong. Yet, if pulses are unobservable in the initial RATAN-600 recording, the source is outside of the radar beam. The converse is false. If we see bursts in the RATAN-600 recording, and not in the integral flux at BBMS, then the latter has insufficient flux sensitivity.

It is possible to localize the drifting burst source on the solar disk if we know the source shift from the preflare position of the continual source and refer 1D data to the SSRT radio map at 5.7 GHz. In the event under study, we determined the first coordinate from EW array data; the second, from RATAN-600 data.

Figure 4 illustrates the localization of the pulse source at 5.7 GHz from 1D data. First, we fix the position of a preflare source. The left part of Figure 4 shows the positional relationship of preflare scans from SSRT (red) and RATAN-600 (blue) on the SSRT radio map. The RATAN-600 preflare scan was obtained in azimuth –2, the position angle was 14.7°; the SSRT preflare scan from the EW array was taken before the onset of the flare, the position angle was –43.3°. In each scan, we

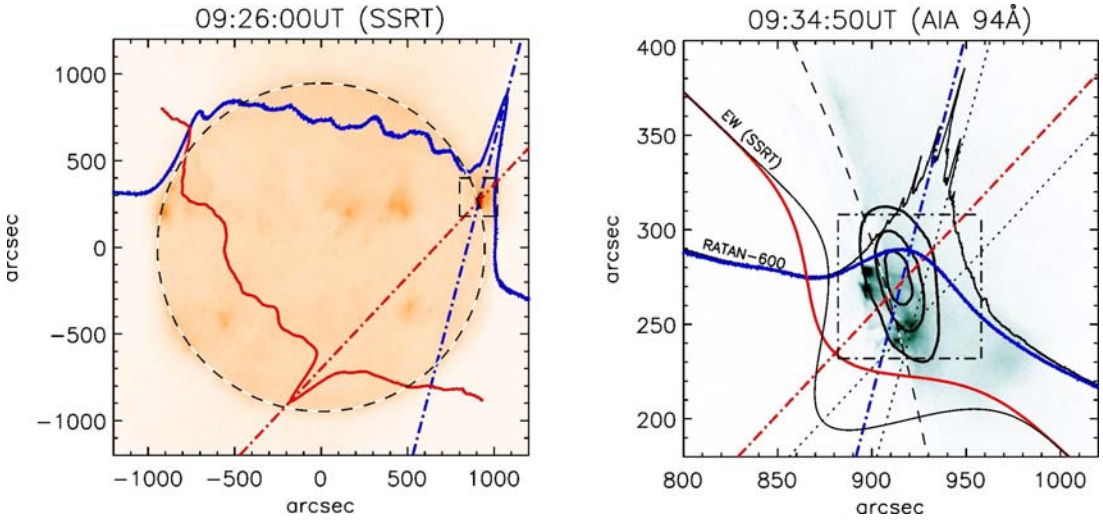

Figure 4. Localization of microwave sources at 5.7 GHz: the continual source (on the left), the drifting burst source (on the right). Preflare scans are marked with colors: SSRT scans are red; RATAN-600 ones, blue. Flare scans are black. The intersection of dash-dot lines indicates the center of radio brightness of the preflare source. The radio map at 5.7 GHz is drawn for 09:26 UT; on the right, the continual source is shown by a contour line. The EUV 94 Å image was captured by SDO/AIA when RATAN-600 registered type III drift microwave bursts. The intersection of dashed lines shows the position of the drifting burst source at 5.7 GHz

superposed the maximum response to the preflare continual source onto the maximum of the source on the radio map. Thus, the intersection of dash-dot perpendiculars to scanning directions defines 2D coordinates of the preflare source.

Then recall that the shift of the drifting burst source at 5.7 GHz from the initial position of the preflare continual source was 20″ according to EW array data (see Figure 2, panel *b*) and 10″ according to RATAN-600 data (see Table). The right part of the figure pictures the positional relationship of preflare (color) and flare scans (black). The background is the UV 94 Å image of the flare region; the contour shows the preflare microwave source at 5.7 GHz. Recall that the RATAN-600 flare scan was taken in azimuth –4 in which we determined the position of the drifting burst source, using the above original method. Thus, the intersection of the dashed lines obtained by dropping respective perpendiculars from flare scans to scanning directions corresponds to the position of the drifting burst source at 5.7 GHz.

DISCUSSION

Altyntsev and Meshalkina [Meshalkina et al., 2002; Altyntsev et al., 2007; Meshalkina et al., 2012] showed that observable type III microwave bursts can occur as clusters.

The scattering of burst positions about the mean within a group proved to be rather low, less than 2–3″, although frequency drift velocities and drift directions were essentially different. At the same time, positions of the groups may differ considerably from cluster to cluster.

Benz et al. [Benz et al., 2002] noted a similar regularity in localization of decimeter spike sources. The authors established that the sources at different frequencies can spatially coincide and be spaced away from each other. If, however, in an event spikes appeared in groups, for one group at a fixed frequency there was one source, but it could differ spatially from a source of another group at the same frequency.

We also examine grouped drifting microwave bursts that occurred in the interval 09:34:40–09:34:50 UT. The two radio telescopes observed the burst source at different position angles; and although it is impossible to localize a source for each burst, we assume that the position of the source of a drifting burst group at a fixed frequency coincides de facto with the position of the source of each burst from the group. This is likely to be valid for such types of fine structures as drifting bursts and spikes, but we cannot extend this regularity to structures of other types regardless of frequency and emission band.

Most of the positively drifting bursts give us grounds for suggesting that the plasma disturbance propagated from loop tops, observed in UV, to their footpoints. Note that we identify the position of the burst source at 5.7 GHz with southern footpoints of two bright loops, seen in UV, at a height of about 1/3 of the loop length (see Figure 4). It is evident that the loops overlap along the line of sight near southern footpoints, thus impeding understanding of the origin of bright cores located near the estimated position of the drifting burst source: it is still unclear whether it is the effect of superposition or of loop interaction.

Figure 5 shows evolution of an active region in UV. We have found out that while the east loop is fixed, the southern part of the west loop moves upward. From the 5th frame, we can see both the underlying fine loop structures and the west loop moving up. The loop interaction is clearly evident in all subsequent frames as a small dark straight area of length no more than 5 ″, tangential to the west loop. Figure 5, on the right, pictures this dark area as a dark-blue source enclosed by two loops. The analysis of the dark area indicates that it moves from the southern footpoint of the west loop to its top; in this case, the dark area lengthens from 5″ in the 6th frame to 10″ in the 10th one. The 13th and 14th frames show disruption and decay of the dark area into two crossing loop structures.

RATAN-600 and BBMS data allowed us to determine 1D positions of drifting burst sources at 4.5, 4.7, 4.9, 5.1, 5.3, 5.5, and 6.0 GHz (Figure 5, on the right).

Here we plot the 1D positions of sources from the following considerations. First, according to the theory of plasma mechanism of microwave radiation, the drifting microwave bursts can occur due to the existence of plasma density gradient both with height and with temperature [Altyntsev et al., 2007].

Second, using SSRT data, Meshalkina and Altyntsev have shown that the drifting burst sources simultaneously observed in two interference orders are displaced by 2–4″ from each other [Meshalkina et al., 2002; Altyntsev et al., 2007; Meshalkina et al., 2012].

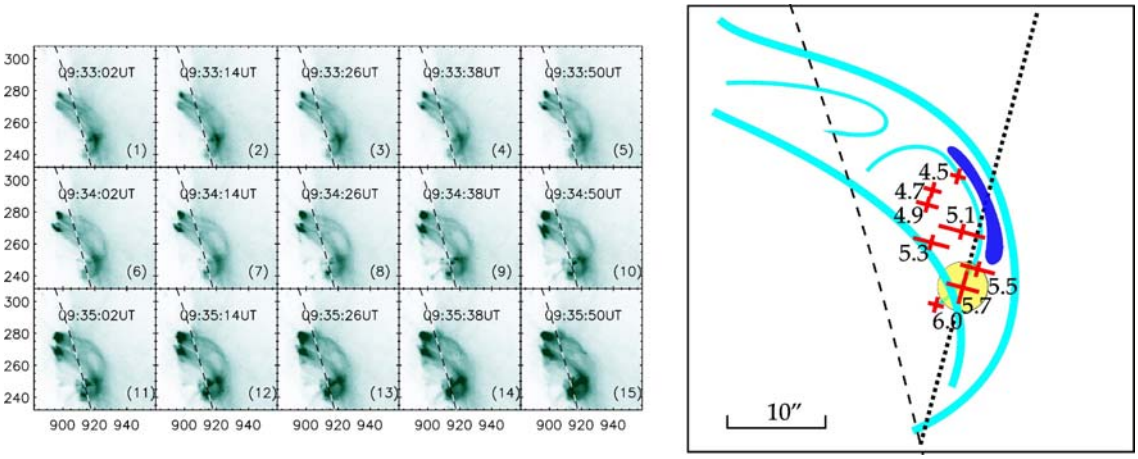

Figure 5. Evolution of the active region during the August 10, 2011 flare in EUV at 94 Å as inferred from AIA data (on the left) and the schematic illustration of the position of microwave drifting burst sources (on the right). We drew the illustration from the 10th frame. The source position at 5.7 GHz is marked with the yellow circle. The dashed line is the RATAN-600 beam axis. Sizes of the microwave sources are indicated by segments orthogonal to the beam axis; for clarity, the sizes are decreased 35 times. The extended drift source seen in the series of UV images is dark blue

Note that we can see adjacent orders at different frequencies and the difference can be as great as 120 MHz.

In our case, the difference between frequencies is 200 MHz. This allows us to estimate possible shifts between sources at adjacent frequencies by the same values, i.e. 2–4″.

Thus, we determine the 1D positions of drifting burst sources over the entire bandwidth of burst occurrence, i.e. from 4.5 to 6 GHz (see Table). Given the 2D position of the drifting burst source at 5.7 GHz and relative shifts of sources at other frequencies, we can localize the emission region. Figure 5 (on the right) introduces a possible scheme for source position at all the frequencies. Presumably the sources localize near the interaction site between rising and stable loops.

According to [Bastian, 1994], scattering of microwave radiation by coronal plasma irregularities leads to an increase in the observed size of a source; and this effect becomes stronger toward the limb. However, Meshalkina and Altyntsev [Altyntsev et al., 1996; Meshalkina et al., 2005] show that adequate interpretation of observed sizes of SSP sources requires spectral data. We found out that at 5.1 GHz the pulse source reached the maximum size relative to the source sizes at other frequencies, i.e. relative to this frequency the response sizes decreased regardless of frequency variations. Notice that at frequencies of 4.5 and 6 GHz, sizes of the sources appeared to be smaller than those of the radar beam.

According to observations of type III bursts at meter and decimeter wavelengths [Reid et al., 2014], sizes of type III burst sources increase with decreasing frequency. On the other hand, Chen et al. [Chen et al., 2013], after studying drifting bursts observed by the updated radio telescope VLA (Very Large Array, USA), reported a case when sizes of the source of a negatively drifting burst increased with increasing

frequency. Analyzing their paper, we concluded that VLA observed the drifting burst in a limited bandwidth. According to the dynamic spectrum, the spectral maximum of the burst was at higher frequencies than the upper working frequency of the receiver; in this case, sizes of the observed response also increased with frequency. Unfortunately, the limited band of receiving frequencies might not have allowed the researchers to find out that the size of the burst source should have decreased with a further increase in frequency – the maximum size of the source might have been determined at the frequency of spectral maximum of the burst.

CONCLUSION

We have localized both the 2D position of the source of the drifting burst at 5.7 GHz and 1D positions of those at seven frequencies (4.5, 4.7, 4.9, 5.1, 5.3, 5.5, and 6.0 GHz), using RATAN-600 and BBMS data. Assuming that emission of drifting bursts at different frequencies originates from different regions and given the exact position of the source at 5.7 GHz, we estimated the geometry of the burst source. The complex analysis of data has revealed that the sources of the type III microwave bursts were located near the region of interaction of UV flare loops. We have established that the source of drifting microwave bursts had its maximum size at 5.1 GHz relative to which the size of effectively emitting region decreased regardless of frequency variations.

Zhdanov D.A. thanks the Russian Foundation for Basic Research for financial support of the work (RFBR grant No. 13–02–90786 mol_rf_nr) and expresses appreciation to Altyntsev A.T. and Fleishman G.D. for helpful comments on this work. We are grateful to referees for discussion and critical comments and to SSRT, RATAN-600, and SDO teams for free access to data. The work was supported the Russian Foundation for Basic Research (№ 15–02–01089, 15–02–03717, 14–02–91157) and Marie Curie PIRSES–GA–2011–295272 project RadioSun.

REFERENCES

Allaart M.A.F., van Nieuwkoop J., Slottje C., Sondaar L.H. Fine structure in solar microwave bursts. *Solar Phys*. 1989, vol. 130, pp. 183.

Altyntsev A.T., Grechnev V.V., Konovalov S.K., Lesovoi S.V., Lisysian E.G., Treskov T.A., Rosenraukh Yu.M., Magun A. On the apparent size of solar microwave spike sources. *Astrophys. J*. 1996, vol. 469, pp. 976.

Altyntsev A.T., Nakajima H., Takano T., Grechnev V., Konovalov S. The study of solar flares with microwave sub-second pulses at 5.7 and 17 GHz. *Proc. Nobeyama Symp.* 1999, pp. 279–282.

Altyntsev A.T., Lesovoi S.V., Meshalkina N.S., Sych R.A., Yan Yihua. The microwave subsecond pulse of September 17, 2001: The spectrum, location and size of the source. *Astron. Astrophys*. 2003, vol. 400, pp. 337–346.

Altyntsev A.T., Grechnev V.V., Meshalkina N.S., Yan Y. Microwave type III-like bursts as possible signatures of magnetic reconnection. *Solar Phys*. 2007, vol. 242, pp. 111.

Bastian T.S. Angular scattering of solar radio emission by coronal turbulence. *Astrophys. J.* 1994, vol. 426, p. 774.

Benz A.O. Millisecond radio spikes. *Solar Phys*. 1986, vol. 104, pp. 99–110.

Benz A.O., Saint-Hilaire P., Vilmer N. Location of narrowband spikes in solar flares. *Astron. Astrophys*. 2002, vol. 383, pp. 678–684.

Bogod V.M., Zhekanis G.N., Mingaliev M.G., Tokhchukova S.Kh. Multi-azimuth regime of observation at RATAN-600 southern sector with periscope reflector. *Izvestiya Vuzov. Radiofizika* [Institute reports. Radiophysics]. 2004, vol. 47, pp. 255. (In Russian).

Bogod V.M. RATAN-600 radio telescope in the 24th solar activity cycle. I. New opportunities and tasks. *Astrophys. Bull.* 2011, vol. 66, pp. 190.

Bogod V.M., Alesin A.M., Pervakov A.A. RATAN-600 radio telescope in the 24th solar-activity cycle. II. Multi-octave spectral and polarization high-resolution solar research system. *Astrophys. Bull.* 2011, vol. 66, pp. 205.

Bruggmann G., Magun A., Benz A.O., Stehling W. Solar flare microwave observations with high spectral resolution. *Astron. Astrophys.* 1990, vol. 240, pp. 506–510.

Chen B., Bastian T.S., White S.M., Gary D.E., Perley R., Rupen M., Carlson B. Tracing electron beams in the Sun's corona with radio dynamic imaging spectroscopy. *Astrophys. J. Lett.* 2013, vol. 763, pp. L21.

Chernov G.P., Yan Y.H., Fu Q.J. A superfine structure in solar microwave bursts. *Astron. Astrophys.* 2003, vol. 406, pp. 1071–1081.

Chernov G.P., Yan Y.H, Fu Q.J. The importance of source positions during radio fine structure observations. *Res. Astron. Astrophys.*. 2014, vol. 14, pp. 831–842.

Droege F. Millisecond fine-structures of solar burst radiation in the range 0.2–1.4 GHz. *Astron. Astrophys.* 1977, vol. 57, pp. 285–290.

Fu Q., Qin Z., Ji H., Pei L. A broadband spectrometer for decimeter and microwave radio bursts. *Solar Phys.* 1995, vol. 160, pp. 97.

Fu Qi-Jun, Yan Yi-Hua, Liu Yu-Ying, Wang Min, Wang Shu-Juan. A new catalogue of fine structures superimposed on solar microwave bursts. *Chinese J. Astron. Astrophys.* 2004, vol. 4, pp. 176–188.

Gary D.E. Hurford G.J., Nita G.M., White S.M. McTiernan J., Fleishman G.D. The Expanded Owens Valley Solar Array (EOVSA). *Bull. Am. Astron. Soc.* 2014, vol. 224, pp. 123.

Grechnev V.V., Lesovoi S.V., Smolkov G.Y., Krissinel B.B., Zandanov V.G., Altyntsev A.T., Kardapolova N.N., Sergeev R.Y., Uralov A.M., Maksimov V.P., Lubyshev B.I. The Siberian Solar Radio Telescope: The current state of the instrument, observations, and data. *Solar Phys*. 2003, vol. 216, pp. 239–272.

Huang J., Yan Y., Liu Y. The statistical features of radio bursts with fine structure at 1.1–7.6 GHz. *Adv. Space Res.* 2010, vol. 46, pp. 1388–1393.

Jiricka K., Karlicky M. Meszarosova H., Snizek V. Global statistics of 0.8–2.0 GHz radio bursts and fine structures observed during 1992–2000 by the Ondrejov radiospectrograph. *Astron. Astrophys.* 2001, vol. 375, pp. 243–250.

Kashapova L.K., Tokhchukova S.K., Rudenko G.V., Bogod V.M., Muratov A.A. On the possible mechanisms of energy release in a C-class flare. *Central European Astrophys. Bull.* 2013, vol. 37, pp. 573–583.

Kashapova L.K., Tokhchukova S.K., Zhdanov D.A., Bogod V.M., Rudenko G.V. The subsecond pulses during the August 10, 2011 flare by observations of RATAN-600 and the 4–8 GHz Siberian solar spectropolarimeter. *Geomagnetism and Aeronomy.* 2013, vol. 53, pp. 1021–1024.

Khaikin S.E., Kaidanovsky N.L., Pariisky Yu.N., Esepkina N.A. RATAN–600 Radiotelescope. *Izvestiya Glavnoi Astronomicheskoi Observatorii v Pulkove* [The Central Astron. Observatory Rep.]. 1972, vol. 188, pp. 3–12. (In Russian).

Lesovoi S.V., Altyntsev A.T., Ivanov E.F., Gubin A.V. A 96-antenna radioheliograph. *Res. Astron. Astrophys.* 2014. vol. 14, pp. 864–868.

Meshalkina N.S., Altyntsev A.T., Grechnev V.V., Sych R.A., Yihua Y. An analysis of the spatial features of drifting bursts in the microwave range. *ESA Special Publication*. 2002. vol. 506, pp. 343–346.

Meshalkina N.S., Altyntsev A.T., Sych R.A., Chernov G.P., Yihua Y. On the wave mode of subsecond pulses in the cm-range. *Solar Phys.* 2004. vol. 221. pp. 85–99.

Meshalkina N.S. Altyntsev A.T., Lesovoy S.V., Zandanov V.G. On the size of solar microwave subsecond impulse sources. *Solnechno-Zemnaya Fizika* [Solar-Terr. Phys.]. 2005, vol. 8, pp. 82–84 (in Russian).

Meshalkina N.S. Altyntsev A.T., Zhdanov D.A., Lesovoi S.V., Kochanov A.A., Yan Y.H., Tan C.M. Study of flare energy release using events with numerous type III-like bursts in microwaves. *Solar Phys.* 2012, vol. 280, pp. 537–549.

Nakajima H., Nishio M., Enome S., Shibasaki K., Takano T., Hanaoka Y., Torii C., Sekiguchi H., Bushimata T., Kawashima S. The Nobeyama Radioheliograph. *IEEE Proc.* 1994, vol. 82, pp. 705–713.

Reid H.A.S., Ratcliffe H. A review of solar type III radio bursts. *Res. Astron. Astrophys.* 2014, vol. 14, no. 7, pp. 773–804.

Staehli M., Benz A.O. Microwave emission of solar electron beams. *Astron. Astrophys.* 1987, vol. 175, pp. 271–276.

Sych R. A., Altyntsev A. T., Grechnev V.V., Meshalkina N.S., Yan Y. Observations of microwave subsecond pulses with high spectral and spatial resolution. *ESA Special Publ.* 2002, pp. 761.

Tokhchukova S. Kh., Korzhavin A. N., Bogod V. M., Kurochkin E. A., Shendrik A. V. Computing the horizontal size of the RATAN-600 beam for the «Southern sector with a flat reflector» mode with allowance for parameters of primary reflectors. *Astrofizicheskii Byulleten'* [Astrophys. Bull.]. 2014, vol. 69, iss. 3, pp. 337–388. (In Russian).

Yan Y., Wang W., Liu F., Geng L., Chen Z., Zhang J. Radio imaging spectroscopy observations of the Sun in decimetric and centimetric wavelengths. *IAU Symp*. 2013, vol. 294, pp. 489–494.

Zhdanov D. A., Zandanov V. G. Broadband microwave spectropolarimeter. *Central European Astrophys. Bull.* 2011. vol. 35, pp. 223–228.

Zhdanov D.A., Zandanov V.G. Observations of microwave fine structures by the Badary Broadband Microwave Spectropolarimeter and the Siberian Solar Radio Telescope. *Solar Phys.* 2015, vol. 290, no. 2, pp. 287–294.